Solid State Ionics 180 (2009) 1285–1289

Contents lists available at ScienceDirect

Solid State Ionics

journal homepage: www.elsevier.com/locate/ssi

Improving $La_{0.6}Sr_{0.4}Co_{0.2}Fe_{0.8}O_{3-\delta}$ cathode performance by infiltration of a $Sm_{0.5}Sr_{0.5}CoO_{3-\delta}$ coating

Xiaoyuan Lou, Shizhong Wang, Ze Liu, Lei Yang, Meilin Liu *

Center for Innovative Fuel Cell and Battery Technologies, School of Materials Science and Engineering, Georgia Institute of Technology, Atlanta, GA 30332-0245, USA

ARTICLE INFO

Article history:
Received 21 December 2008
Received in revised form 21 May 2009
Accepted 25 June 2009

Keywords:
Solid oxide fuel cell
LSCF
SSC
Cathode modification
Infiltration

ABSTRACT

$La_xSr_{1-x}Co_yFe_{1-y}O_{3-\delta}$ (LSCF) represents one of the state-of-the-art cathode materials for solid oxide fuel cells (SOFCs) due primarily to its high ionic and electronic conductivity. In this study, a one-step infiltration process has been developed to deposit, on the surface of a porous LSCF cathode, a thin film (50–100 nm) of $Sm_{0.5}Sr_{0.5}CoO_{3-\delta}$ (SSC), which is catalytically more active for oxygen reduction. Electrochemical impedance spectroscopy reveals that the SSC coating has dramatically reduced the polarization resistance of the cathode, achieving area-specific resistances of 0.036 Ω cm^2 and 0.688 Ω cm^2 at 750 °C and 550 °C, respectively. It has also maintained the stability of LSCF cathodes. In particular, the peak power densities are increased by ~22% upon the infiltration of SSC onto the porous LSCF cathodes of our best performing cells. These results demonstrate that a conductive backbone (e.g., LSCF) coated with a catalytic film (e.g., SSC) is an attractive approach to achieving an active and stable SOFC cathode for low-temperature solid oxide fuel cells.

1. Introduction

One of the critical challenges facing the development of a new generation of solid oxide fuel cells (SOFCs) is to develop novel electrode and electrolyte materials for the operation at sufficiently low temperatures to dramatically reduce the cost and improve the reliability and operational life [1,2]. The cathode, in particular, represents an important area of current SOFC research and development since most of the power losses arise from the cathode relevant to the oxygen reduction, more so at lower operating temperatures [3–6].

Cathode materials in the family of strontium- and iron-doped lanthanum cobaltite, $La_xSr_{1-x}Co_yFe_{1-y}O_{3-\delta}$ (LSCF), are considered state-of-the-art for the YSZ-based SOFCs, although a doped-CeO_2 buffer layer must be used to prevent any undesirable reactions between LSCF and YSZ [7]. LSCF exhibits a much higher performance than the conventional cathode, $La_xSr_{1-x}MnO_{3-\delta}$ (LSM), due primarily to its excellent ionic and electronic conductivity, significantly extending the active zones for the oxygen reduction (e.g., far beyond the three-phase-boundary of LSM) [8,9]. Unfortunately, LSCF cathode exhibits a degradation of performance over time, more so at higher operating temperatures [10].

$Sm_{0.5}Sr_{0.5}CoO_{3-\delta}$ (SSC) is considered an excellent cathode especially at low temperatures. It has a much higher surface oxygen exchange rate [11,12] and bulk oxygen ion diffusion coefficient [12] than LSCF. However, samarium is expensive and its use in large amounts may not be cost competitive. Also, it should be noted that SSC is reactive when fired directly on an YSZ electrolyte [13], potentially creating a long-term instability. Thus, the development of cathodes with high activity and stability is still a key challenge. Considering the time-consuming design and optimization process for the development of new electrode materials, an effective way is to modify the existing cathode materials for high performance. Extensive studies have been done to optimize the LSCF-based cathodes for future commercialization. Infiltration (or impregnation) is an effective method to introduce a thin film of the catalyst onto a porous supporting structure [14]. It has been widely used to fabricate the electrodes for the polymer electrolyte membrane fuel cells [15]. Recently, it has been reported that both the cathode and anode performances in SOFCs can be significantly improved by infiltrating various materials [16–22]. With the help of the infiltrated materials in the porous structures, the surface properties can be improved by adjusting the local oxygen ion and electron conductivity, as well as the electro-catalytic properties. For example, the Berkeley group has shown that the performance of an LSCF-based cathode can be enhanced by infiltrating nanoparticles of $Y_{0.2}Ce_{0.8}O_{1.9}$ (YDC) into an LSCF porous backbone [19].

Here we report the findings of our investigation into an SSC-infiltrated LSCF cathode — a porous LSCF backbone (with high ionic and electronic conductivity) coated with a thin layer of SSC nano coating (with high catalytic activity toward O_2 reduction) through a one-step infiltration process. We have demonstrated that the performance of an advanced LSCF cathode can be significantly enhanced by an SSC coating without losing the stability, using both the symmetrical cells and fuel cells.

* Corresponding author. Tel.: +1 404 894 6114; fax: +1 404 894 9140.
E-mail address: meilin.liu@mse.gatech.edu (M. Liu).

0167-2738/$ – see front matter © 2009 Elsevier B.V. All rights reserved.
doi:10.1016/j.ssi.2009.06.014

2. Experimental

2.1. Symmetric cell preparation

The $Gd_{0.1}Ce_{0.9}O_{1.95}$ (GDC) pellets were prepared by uniaxially pressing the commercial GDC powder (from Rhodia). The pellets were sintered at 1450 °C for 5 h, resulting in a relative density of ~98%. Iron-rich LSCF ($La_{0.6}Sr_{0.4}Co_{0.2}Fe_{0.8}O_{3-\delta}$) powder with an average particle size of ~100 nm was prepared using the citrate method. Mixed with V006 thinner (from Heraeus) and acetone under a ratio of 2:1:1, LSCF slurry was made after 2-h ball-milling. LSCF|GDC|LSCF symmetric cell was then fabricated by screen-printing LSCF slurry on both sides of the GDC pellet with a similar thickness (around 30 μm). Porous LSCF electrodes were finally obtained by sintering at 1080 °C for 2 h.

2.2. Infiltration

Aqueous nitrate solutions of the SSC precursor with 0.16, 0.48 and 1.44 mol/L were prepared by mixing $Sm(NO_3)_3 \cdot 6H_2O$, $Sr(NO_3)_2$, $Co(NO_3)_2 \cdot 6H_2O$ and urea with corresponding molar ratios. 0.48 mol/L LSCF precursor was also prepared for comparison by mixing $La(NO_3)_3 \cdot 6H_2O$, $Sr(NO_3)_2$, $Co(NO_3)_2 \cdot 6H_2O$, $Fe(NO_3)_3 \cdot 6H_2O$ and urea. Urea acted as a complex agent to form the correct perovskite phase. Ethanol was added into the aqueous solution with a ratio of 0.6:1 to improve the wetting ability on the LSCF backbone. 7 μl of this solution was then infiltrated into each side of the porous LSCF electrode using a micro-liter syringe in order to control the amount of loading. Vacuum apparatus was employed to force the liquid into those micro pores. Pt wires were attached to the electrolyte on one side of the symmetric cell as the reference electrodes. After the infiltration, the cell was fired at 800 °C for 1 h to obtain a right phase. For the X-ray diffraction (XRD) characterization, identical nitrate solutions were also fired to the powder under the same condition. A blank cell without infiltration was also tested for comparison.

2.3. Electrochemical testing

Two 100 mesh Pt grids were attached and spring-pressed on both sides of the symmetric cell as the current collectors. Polarization was applied using another Pt wire as a reference electrode. The sample was held by a quartz sample holder and exposed to 100 ml min^{-1} flowing air. The impedance spectra were acquired under open-circuit voltage (OCV) using a Potentiostat (Solartron 1287) and a frequency analyzer (Solartron 1255) interfaced with a computer, with an applied *ac* voltage of 5 to10 mV in the frequency range from 0.01 Hz to 10 MHz. Test cells with and without the infiltration of SSC were operated at a constant current density of 235 mA/cm^2 for 100 h to evaluate the stability of cathode performance. Impedance spectra of the cells were also acquired intermittently during the cell operation to determine the changes in interfacial polarization resistance in addition to continuous monitoring of the changes in cell voltage.

2.4. Infiltration and testing of high-performance button cells

To confirm the observed catalytic effect, we also infiltrated 3 μL 1.44 mol/L SSC ethanol/water solution into the porous LSCF cathodes of the high-performance button cells, using the same procedures as described earlier. The active electrode area was ~0.3 cm^2. A Pt mesh was attached to cathode with a minimum amount of Pt paste. The cell was then mounted on an alumina supporting tube, followed by firing at 850 °C for 2 h to ensure the formation of a proper SSC phase. The temperature was subsequently reduced to 700 °C for the fuel cell testing with the humidified hydrogen (3 vol.% H_2O) as a fuel and the ambient air as an oxidant.

2.5. Physical characterization

Phase identification was carried out on an X'Pert PRO Alpha-1 X-ray diffractometer using a Cu Kα radiation. Microstructures were characterized using a LEO 1530 thermally-assisted field emission scanning electron microscope.

3. Results and discussion

3.1. Phase formation and chemical compatibility

Shown in Fig. 1 are the XRD patterns of LSCF and SSC powders derived from the solutions prepared for the infiltration. The desired perovskite phase is obtained for both samples under the conditions for the electrode modification by infiltration. Surfactants usually play an important role in the phase and structure formation of a solution-based synthesis [23]. Our results indicated that Triton X-100 and X-45 were not suitable for the infiltration of a thin coating of SSC and LSCF into a porous LSCF structure. Instead, urea is a better surfactant for this application. To investigate the chemical compatibility between SSC and LSCF, we prepared the mixtures of SSC and LSCF (50:50 wt.%) fired separately at 850, 950, and 1050 °C for 5 h. The same physical mixture without firing was also examined for comparison. As shown in Fig. 2, the characteristic peaks of both SSC and LSCF are clearly separated and identified for the mixture fired at 850 °C; there were no new peaks in

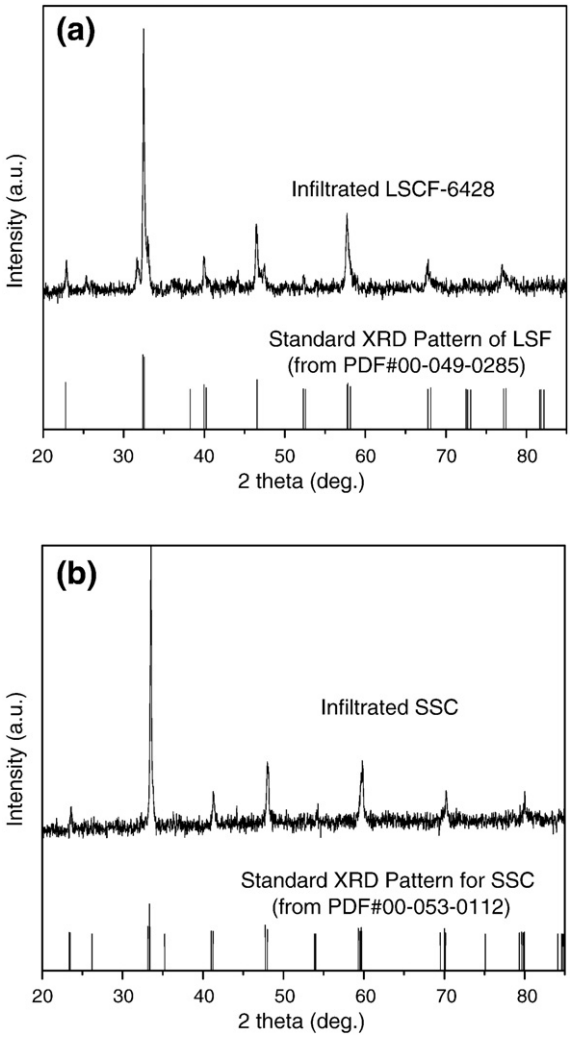

Fig. 1. XRD patterns of infiltrated materials after firing at 850 °C for 2 h: (a) LSCF; (b) SSC.

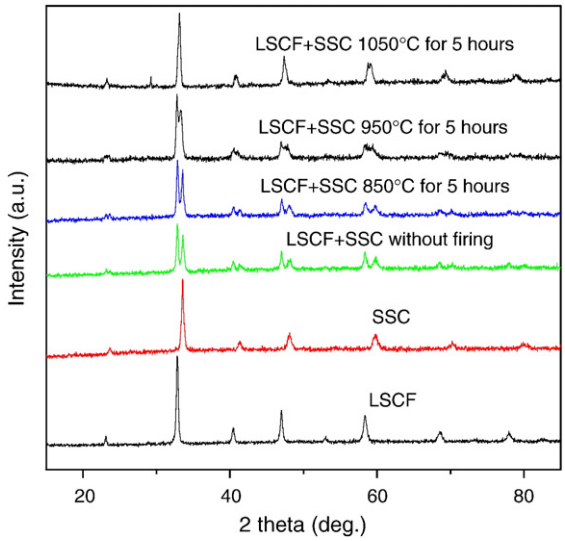

Fig. 2. XRD analysis of LSCF and SSC mixture with and without firing at various temperatures for 5 h.

the XRD pattern. For the mixture fired at 950 °C, however, the peaks of LSCF and SSC shifted towards each other, implying some doping between them. With the further increase in the firing temperature, interaction between LSCF and SSC became apparent for the mixture fired at 1050 °C. These results suggest that SSC and LSCF have a good chemical compatibility at temperatures up to ~850 °C, suggesting that SSC and LSCF are compatible at temperatures below 850 °C.

3.2. Microstructure characteristics

Fig. 3 shows some typical morphologies of LSCF cathodes infiltrated with different concentrations of SSC and LSCF. Initial experiments showed that the wetting ability of water on a perovskite cathode (e.g. LSCF) was not as good as on a fluorite electrolyte (e.g. YSZ). Thus, reducing the surface tension between the precursor solution and the backbone is critical to obtain a continuous coating on the cathode backbone. Organic solvents, such as ethanol and acetone, have much lower surface tensions than water. In this study, a mixture of ethanol and water was used to improve the wetting of the SSC solution on LSCF by considering both water miscibility and boiling temperature. Shown in Fig. 3a is the image of an unmodified blank LSCF backbone, with an average grain size of ~200 nm. Before the infiltration, the surface is clean and the grain boundaries are clearly visible. Shown in Fig. 3b is the image of an LSCF cathode infiltrated with a 0.16 mol/L SSC solution; an SSC catalyst layer was uniformly coated on the surfaces of the LSCF grains. A small amount of SSC nanoparticles (~30 nm in diameter) nucleated from the SSC surface coating due to the saturated loading. This image clearly shows the formation of nanoparticles from a smooth surface coating. For the LSCF infiltrated with the 0.48 mol/L SSC solution, more SSC nanoparticles appeared on the surface of LSCF grains (Fig. 3c). Underneath the particles, a thin film of SSC is visible. The average particle size was around 50 nm. A higher concentration loading of SSC promoted the nucleation and growth rates of those nanoparticles. Fig. 3d shows, by increasing the concentration of SSC to 1.44 mol/L, both

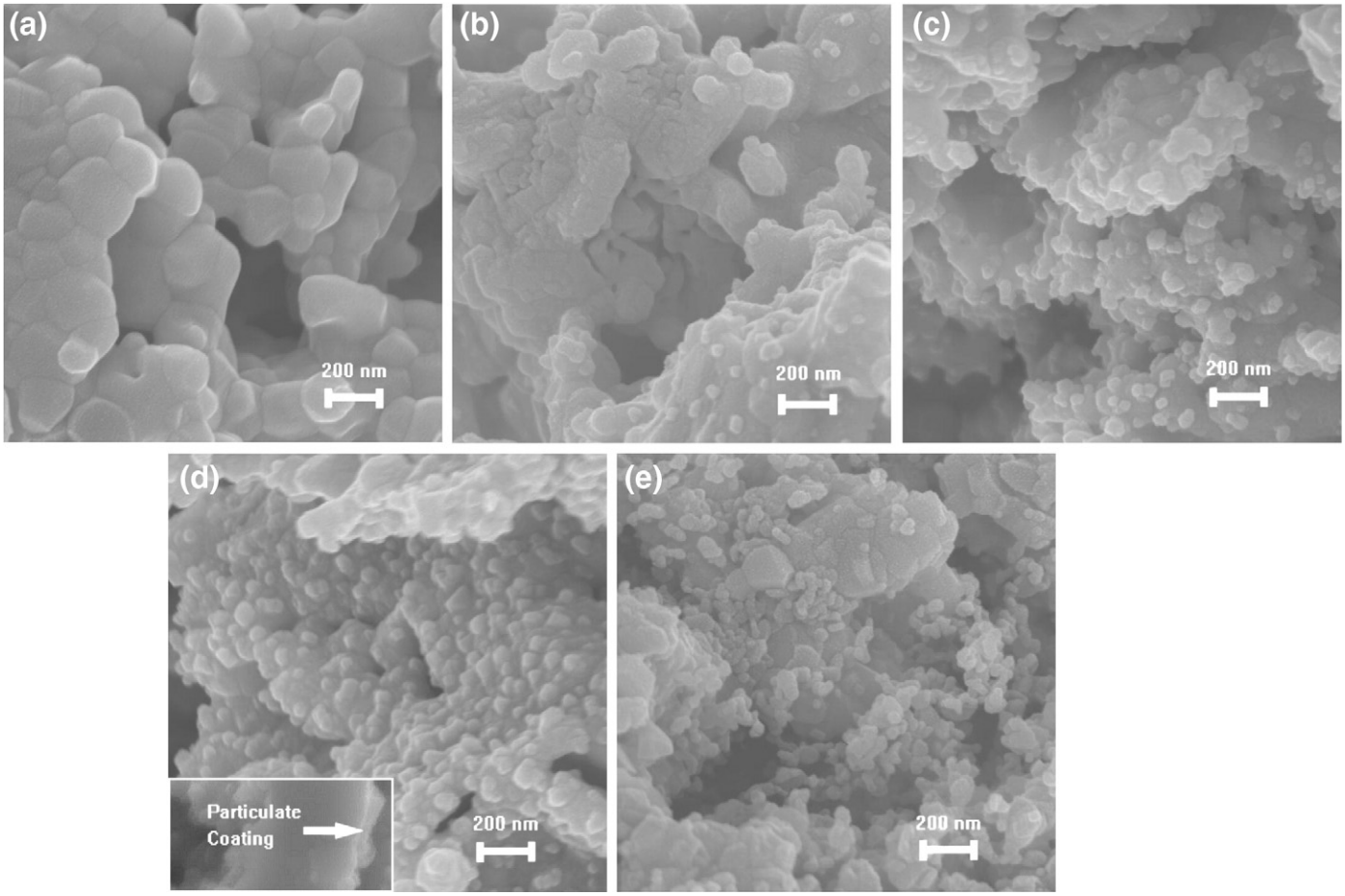

Fig. 3. SEM images of the cross-section of LSCF cathodes: (a) blank LSCF; (b) 0.16 mol/L SSC infiltration; (c) 0.48 mol/L SSC infiltration; (d) 1.44 mol/L SSC infiltration; (e) 0.48 mol/L LSCF infiltration.

nanoparticle amount and size continued to increase. Majority of the grain surface was covered by a layer of SSC particulate coating. Continuous coating provided a strong bonding between SSC layer and LSCF grain to avoid further agglomeration during testing. The average particle size was around 80 nm. The LSCF backbone grain boundary was not visible due to the coverage of the continuous SSC thin film. As shown in the inset, the thickness of particulate film was around 50–100 nm. Fig. 3e reveals the morphology of an LSCF electrode infiltrated with 0.48 mol/L LSCF nitrate solution. The average size of the LSCF particles for the LSCF infiltrated cathode is similar to that of the SSC particles for the SSC-infiltrated cathode for a similar loading of solution. However, the LSCF particles seem to show a stronger tendency for clustering.

3.3. Cathode electrochemical performances

Shown in Fig. 4 are the impedance spectra of several infiltrated cathodes measured at different temperatures at open-circuit voltage (OCV). Each spectrum was collected after the cell reached a steady state (after ~1 h operation). Bulk resistances of these cells were all close to the values estimated from the ionic conductivity and geometry of the electrolyte (the differences were within experimental error). In order to clearly show the differences in the electrode polarization behavior, all bulk resistances were removed from the spectra, showing only the interfacial polarization impedances. As can be seen in Fig. 4a, the blank LSCF cell exhibited an area-specific resistance (ASR) of ~0.103 Ω cm^2 at 750 °C, similar to those reported in the literature [24]. The infiltration of a thin film of LSCF into the porous LSCF electrode reduced the polarization resistance to ~0.071 Ω cm^2, due mainly to an increase in surface area from the nanoparticles as shown in Fig. 3e. In contrast, the cells with SSC-infiltrated LSCF electrodes displayed a much better performance. The interfacial resistances were reduced to about 0.047, 0.043, and 0.036 Ω cm^2, respectively, for the infiltration of 7 μL of 0.16, 0.48, and 1.44 mol/L SSC solution into the porous LSCF electrodes. The dramatic decrease in the electrode polarization resistance is attributed mainly to the enhancement of the surface catalytic properties by the SSC coating. It can be seen from the impedance spectra at 750 °C for the SSC-infiltrated LSCF electrodes that there appear two arcs in the frequency range studied. While the one centered around 1 kHz (high frequency) changed dramatically with the catalyst loading, the other one centered around 10 Hz (low frequency) remained relatively constant. For LSCF-based cathodes, previous studies indicated that the high-frequency arc was usually related to the charge-transfer while the low-frequency one was relevant to the mass-transfer [24]. Thus, the impedance data suggests that the SSC infiltration enhanced the rate of surface oxygen reduction without affecting the transport of oxygen molecules through the porous electrodes. At lower temperatures such as 650 °C and 550 °C (in Fig. 4b,c), the SSC-infiltrated LSCF electrodes also demonstrated better performances than the blank LSCF electrode without infiltration. At 550 °C, the LSCF electrode infiltrated with 1.44 mol/L SSC solution had an electrode polarization resistance of 0.688 Ω cm^2, presenting the best performance among all LSCF-based cathodes ever reported [24,25]. The performance enhancement of SSC infiltration is more pronounced at lower temperatures because of its higher electro-catalytic activity; for example, the 1.44 mol/L SSC infiltration produced a 66.7% decrease in the electrode polarization resistance at 750 °C and an 80.6% decrease at 550 °C.

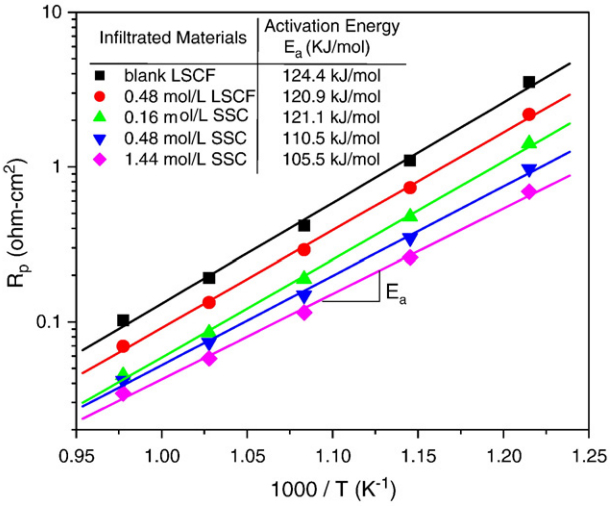

Fig. 5. Interfacial resistances and activation energies as determined from impedance spectra.

It is also noted that the blank LSCF cathode, together with the LSCF infiltrated one, had the highest activation energies among all the LSCF

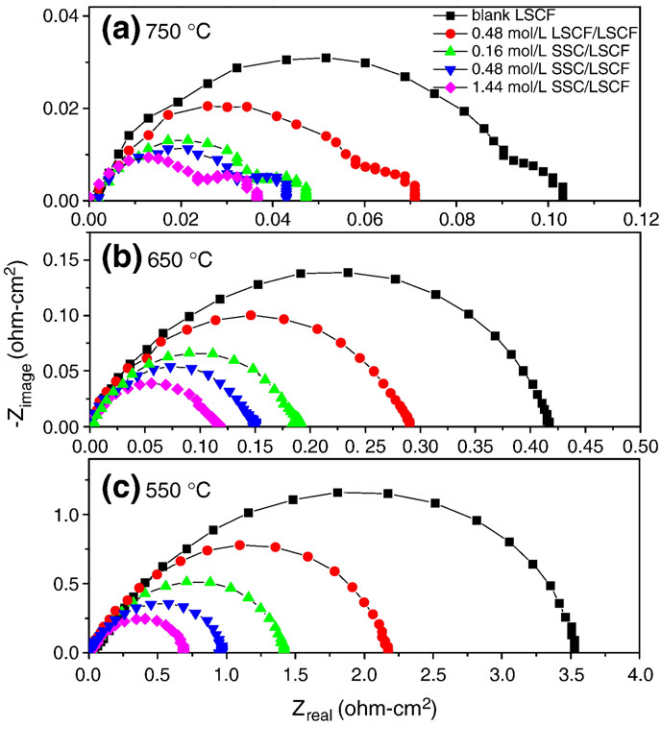

Fig. 4. Impedance spectra of LSCF cathodes with different treatments at various temperatures: (a) 750 °C; (b) 650 °C; (c) 550 °C.

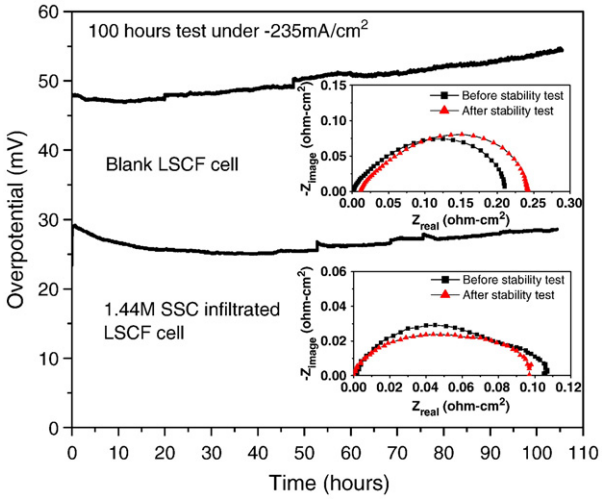

Fig. 6. Comparison of 100 h stabilities between blank LSCF cathode and 4 μL 1.44 mol/L SSC-infiltrated LSCF cathode under constant current density of 235 mA/cm^2 at 700 °C.

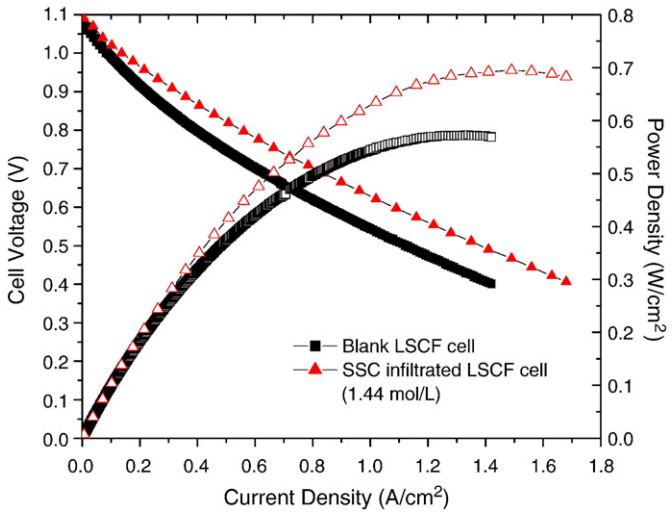

Fig. 7. Cell voltages (solid symbols) and power densities (open symbols) as a function of current densities for blank and SSC-infiltrated LSCF fuel cells operated at 700 °C.

electrodes studied, as shown in Fig. 5. The activation energy decreased with increasing SSC loading within the range of catalyst loading studied.

3.4. Cell stability of SSC-infiltrated cathodes

Fig. 6 shows the performances of a blank cell and an SSC-infiltrated cell operated at a constant current density of 235 mA/cm^2 at 700 °C for 100 h. The overpotential of the blank LSCF cathode suffered around 13% degradation. Similar to a previous study [10], impedance measurements showed both bulk and interfacial resistances increased after the 100-h testing. However, the SSC infiltration not only significantly reduced the cathode overpotential but also maintained the cell stability over a 100-h operation. The impedance of the cell remained relatively constant, as seen from the impedance spectra acquired before and after the 100-h operation. While a long-term performance degradation of catalysts is usually associated with the agglomeration of the nanoparticles of catalysts or the new phase formation due to the reactions between the catalysts and backbone materials [26,27], post analysis of the SSC-infiltrated LSCF cathodes using SEM showed no evidence of the particle agglomeration. The SSC catalytic layer on the surface of the LSCF grains reduced the LSCF degradation rate to some extent within the time range of testing.

3.5. Performance enhancement

To further confirm the catalytic effect of SSC infiltration, we infiltrated the porous LSCF cathode of a high-performance button cell with the SSC solution. Fig. 7 shows the current–voltage curves and power densities for the SSC-infiltrated cell operated at 700 °C, together with those for a blank cell (without SSC infiltration). The open-circuit voltages (OCV) were about 1.08 V for both cells. However, the peak power densities were 572 mW/cm^2 for the blank cell and 695 mW/cm^2 for the infiltrated cell, implying a ~22% increase in the peak power density by the infiltration of a thin film of SSC. It should be noted that this infiltration process can be readily applied to other SOFCs to effectively enhance the fuel cell performance, especially for SOFCs to be operated at intermediate or lower temperatures.

4. Conclusion

A uniform coating of catalytically active SSC has been successfully deposited on the surface of a porous LSCF cathode through the optimization of a one-step solution infiltration process. The performance of the LSCF cathode has been enhanced by a thin layer of SSC coating. The cell degradation was also reduced to some extent within the time range of testing although the detailed mechanism is yet to be determined. The results imply that a conductive backbone (e.g., LSCF) coated with a catalytically active film (e.g., SSC) is an attractive approach to achieving a highly active and stable SOFC cathode for low-temperature solid oxide fuel cells. Further, the methodology may be applicable to other cathode materials with high catalytic activities, but limited stability and compatibility with electrolyte or other cell components.

Acknowledgment

This work was supported by the Department of Energy NETL under grant no. DE-FC26-02NT41572.

References

[1] S.C. Singhal, Solid State Ionics 135 (1–4) (2000) 305.
[2] S.C. Singhal, Solid State Ionics 152 (2002) 405.
[3] Z.P. Shao, S.M. Haile, Nature 431 (7005) (2004) 170.
[4] C.R. Xia, M.L. Liu, Adv. Mater. 14 (7) (2002) 521.
[5] Y.L. Zhang, S.W. Zha, M.L. Liu, Adv. Mater. 17 (4) (2005) 487.
[6] Y. Liu, S.W. Zha, M.L. Liu, Chem. Mater. 16 (2004) 3502.
[7] S.P. Jiang, Solid State Ionics 146 (1–2) (2002) 1.
[8] J. Fleig, J. Power Sources 105 (2) (2002) 228.
[9] M.L. Liu, J. Electrochem. Soc. 145 (1) (1998) 142.
[10] S.P. Simner, M.D. Anderson, M.H. Engelhard, J.W. Stevenson, Electrochem. Solid-State Lett. 9 (10) (2006) A478.
[11] F.S. Baumann, J. Fleig, G. Cristiani, B. Stuhlhofer, H.U. Habermeier, J. Maier, J. Electrochem. Soc. 154 (9) (2007) B931.
[12] H. Fukunaga, M. Koyama, N. Takahashi, C. Wen, K. Yamada, Solid State Ionics 132 (3–4) (2000) 279.
[13] L. Yang, C.D. Zuo, S.Z. Wang, Z. Cheng, M.L. Liu, Adv. Mater. 20 (17) (2008) 3280.
[14] B. Kasemo, S. Johansson, H. Persson, P. Thormahlen, V.P. Zhdanov, Top. Catal. 13 (1–2) (2000) 43.
[15] S.J. Lee, S. Mukerjee, J. McBreen, Y.W. Rho, Y.T. Kho, T.H. Lee, Electrochim. Acta 43 (24) (1998) 3693.
[16] S.P. Jiang, Mater. Sci. Eng., A 418 (1–2) (2006) 199.
[17] S.P. Jiang, S. Zhang, Y.D. Zhen, A.P. Koh, Electrochem. Solid-State Lett. 7 (9) (2004) A282.
[18] S.D. Park, J.M. Vohs, R.J. Gorte, Nature 404 (6775) (2000) 265.
[19] T.Z. Sholklapper, H. Kurokawa, C.P. Jacobson, S.J. Visco, L.C. De Jonghe, Nano Lett. 7 (7) (2007) 2136.
[20] T.Z. Sholklapper, C. Lu, C.P. Jacobson, S.J. Visco, L.C. De Jonghe, Electrochem. Solid-State Lett. 9 (8) (2006) A376.
[21] A. Atkinson, S. Barnett, R.J. Gorte, J.T.S. Irvine, A.J. McEvoy, M. Mogensen, S.C. Singhal, J. Vohs, Nat. Mater. 3 (1) (2004) 17.
[22] R.J. Gorte, S. Park, J.M. Vohs, C.H. Wang, Adv. Mater. 12 (19) (2000) 1465.
[23] M. Mamak, G.S. Metraux, S. Petrov, N. Coombs, G.A. Ozin, M.A. Green, J. Am. Chem. Soc. 125 (17) (2003) 5161.
[24] E.P. Murray, M.J. Sever, S.A. Barnett, Solid State Ionics 148 (1–2) (2002) 27.
[25] S.B. Adler, Chem. Rev. 104 (2004) 4791.
[26] T.Z. Sholklapper, V. Radmilovic, C.P. Jacobson, S.J. Visco, L.C. De Jonghe, Electrochem. Solid-State Lett. 10 (4) (2007) B74.
[27] W.S. Wang, M.D. Gross, J.M. Vohs, R.J. Gorte, J. Electrochem. Soc. 154 (5) (2007) B439.